

https://doi.org/10.1070/QEL17967

Agar phantoms of biological tissue for fluorescence monitoring of photodynamic therapy

A.V. Khilov, V.A. Shishkova, E.A. Sergeeva, D.A. Kurakina, M.Yu. Kirillin

Abstract. **An approach to fabricating agar phantoms mimicking spectral optical properties of biological tissues with fluorescent inclusions is proposed, which allows one to imitate the problem of optical visualisation of superficial biological tissues after the administration of a chlorin-based photosensitiser. The different arrangement of a fluorescent layer within a phantom makes it possible to simulate biological tissue in the cases of both topical application and intravenous injection of a photosensitiser. It is shown that absorption and scattering spectra of phantoms are in good agreement with the spectra of real biological tissues in the wavelength range of 500–800 nm. Changes in spectra of absorption and scattering coefficients of phantoms, as well as in their fluorescent properties induced by the addition of a fluorescent marker (chlorin-based photosensitiser) are demonstrated.**

Keywords: *optical properties of biotissues, spectroscopy, fluorescence imaging, biotissue phantoms, inverse Monte Carlo technique, photodynamic therapy, chlorin-based photosensitisers.*

1. Introduction

Fluorescence imaging techniques are a promising area of modern optical imaging due to the high contrast of images provided by spectral selection of signals from fluorescent markers, whose emission peaks are located outside the spectral range of biotissue autofluorescence. Primary applications of fluorescence imaging techniques in modern clinical practice include mapping of biotissue vasculature [1], detection of sentinel lymph nodes [2], and monitoring of the local concentration of a photosensitiser (PS) during photodynamic therapy (PDT) [3]. Improvement of modern fluorescence imaging methods and transition from qualitative to quantitative imaging require the development of inexpensive and easily reproducible standards for calibration and validation of the developed techniques. In this regard, a necessary stage consists in fabrication of phantoms that imitate optical properties of basic biotissue in a wide spectral range and its properties after the administration of a fluorescent marker, as well as preserve the specified optical and structural properties for a certain time.

Fat emulsions, such as intralipid [4–6] or its close analogue – lipofundin [7, 8], are traditionally employed as a standard for fabrication of biological tissue phantoms in the visible and near-IR ranges. Intralipid and lipofundin are characterised by different sizes of soybean oil droplets in their composition; however, the difference in their scattering coefficient does not exceed 9% [9]. The optical properties of fat emulsions remain stable over time, in contrast, for example, to milk, which was previously widely employed as a calibration medium [10].

The absorption coefficient of fat emulsions is small [11], since it is primarily determined by absorption of water, which is insignificant in the visible range. In this regard, for development of the phantoms that mimic absorbing properties of real biological tissues, the use of additional chromophores is required. The most accessible and spectrally stable absorbers are India ink [12, 13] and inks of various colours. For example, red ink imitates spectral characteristics of haemoglobin [14]. In paper [15], the values of scattering and absorption coefficients per volume concentration of intralipid and ink at wavelengths of 633 nm, 750 nm, and 830 nm were determined. These values can be chosen as reference values when developing phantoms based on intralipid and ink. It should be noted that phantoms based on fat emulsions are traditionally liquid, which imposes a number of limitations on the fabrication of phantoms with a predefined shape and/or containing inclusions.

For manufacturing semi-solid phantoms of a predefined shape, water with addition of agar [16, 17] is employed, which allows forming stable matrices, to which scattering and absorbing components can be added. The use of agar powder also makes it possible to control optical properties of manufactured biotissue phantoms [18]. In paper [19], an approach to the fabrication of elastic fluorescent phantoms of human skin based on polyacrylamide is proposed, and strict following the manufacturing protocol to preserve the fluorescent properties of the embedded fluorophore is emphasised. It should be noted that typical values of absorption coefficient of the phantoms developed in [19] are significantly lower than those for biotissues in visible spectral range.

In this work, we propose an approach to fabricating agar phantoms that mimic real biotissues, as well as biotissues after administration of chlorin-based PS's widely employed in PDT [20–23]. Spectral properties of human skin of various localisations measured *in vivo* [24] were chosen as reference parameters in the development of the phantoms. The correspondence of scattering and absorption spectra was ensured by adding lipofundin suspension and red ink as a scatterer

A.V. Khilov, E.A. Sergeeva, D.A. Kurakina, M.Yu. Kirillin Institute of Applied Physics, Russian Academy of Sciences, ul. Ulyanova 46, 603950 Nizhny Novgorod, Russia; e-mail: mkirillin@yandex.ru;
V.A. Shishkova Institute of Applied Physics, Russian Academy of Sciences, ul. Ulyanova 46, 603950 Nizhny Novgorod, Russia; Lobachevsky State University of Nizhny Novgorod, prosp. Gagarina 23, 603022 Nizhny Novgorod, Russia

Received 26 November 2021
Kvantovaya Elektronika **52** (1) 63–68 (2022)
Translated by M.Yu. Kirillin

and an absorber, respectively. Fabrication of PS-containing elements was based on the addition of a PS during the liquid phase of the mixture of components. Absorption and scattering spectra of phantoms were demonstrated to be in good agreement with literature data for biological tissues, in particular, for human skin in the range of 500–800 nm [24]; however, they were not in agreement with the superposition of partial spectra of components contained in the phantom. It was also shown that fluorescent properties of the fabricated phantoms are determined by the addition of a fluorescent marker, and not by their intrinsic autofluorescence. The stability (within 10% deviation) of optical properties of the phantoms in the studied wavelength range during long-term storage (1 month) was demonstrated. The proposed approach allows one, in particular, to perform model experiments in the area of PDT planning and monitoring.

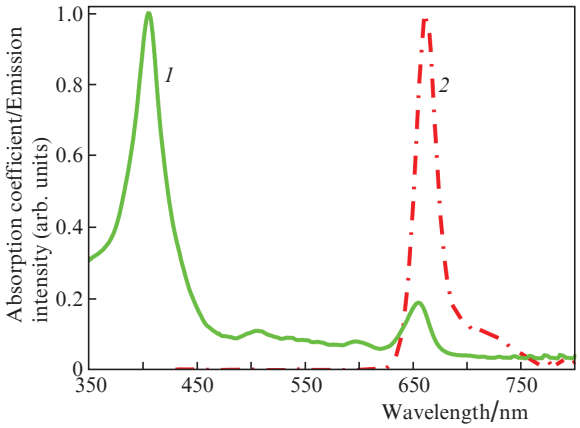

Figure 1. (Colour online) Normalised (*1*) absorption and (*2*) emission spectra of a chlorin-based PS [25].

2. Materials and methods

2.1. Fabrication of agar phantoms of biotissue

An aqueous solution of agar powder with a mass fraction of 1.25% was used as a base matrix. The solution was heated in a microwave oven until a visually observed boiling process (up to a temperature of ~85 °C). Thereafter, the solution was cooled at room conditions with occasional stirring in order to dissolve all the agar powder granules. Lipofundin 20% MCT/LST (Braun, Germany) was mixed with red ink (Koh-i-Noor, Czech Republic) previously subjected to ultrasonication. The use of red ink as the main chromophore of a phantom helps mimic absorption spectrum of biological tissues, which is primarily determined by haemoglobin in the considered wavelength range [14]. The resulting mixture was added to the agar solution cooled to a temperature below 42 °C (protein denaturation temperature). Preliminary experiments have shown that adherence to the specified temperature regime is critical for obtaining a homogeneous phantom. Since it was determined in the experiment that due to the processes occurring in the course of the phantom fabrication, optical properties of the phantom cannot be calculated as a superposition of optical properties of its components, the ratio of the components in the phantom was determined empirically. Volume concentrations of lipofundin and red ink in the resulting solution were 23% and 0.19%, respectively. Resulting solution was then poured into two equal volumes prior to solidification, and a gel-photosensitiser Revixan-Derma (Revixan Ltd., Russia) based on chlorin e6 was added into one of them. The volume concentration of photosensitisers in the resulting fluorescent phantom was 0.1%. The absorption and emission spectra of the PS [25] are shown in Figure 1.

This approach was employed for preparation of solutions for phantoms of basic biotissue and biotissue with administered fluorescent agent, and the differences in optical properties of phantoms were due only to the presence or absence of a PS, which is an additional chromophore according to Fig. 1. Before the solutions solidified, they were poured into cylindrical cells with a diameter of 45 mm with a controlled depth, as well as into rectangular quartz cuvettes with the thickness of 2 mm, aimed for spectrophotometric measurements.

The fabricated phantoms had a cylindrical shape. The thicknesses of the phantoms corresponded to the set of cell depths and equalled 0.51, 0.68, 1.00, and 2.00 mm. The choice of thickness was determined by the typical thicknesses of skin layers and estimations of the depth of chlorin-based PS localisation after different types of administration prior to PDT procedure [25]. In addition, phantoms with the thickness of 30 mm were produced, imitating thick samples of biotissue and also having a cylindrical shape. All fabricated phantoms were packed in an airtight film, placed in a fridge, and then cooled to a temperature of 4 °C to ensure their longer stability during measurements.

The produced set of phantoms allowed one to imitate not only single-layer, but also multilayer biotissues, separate layers of which may contain a fluorophore. The location of the fluorescent layer above the base phantom layer simulates the situation of topical application of fluorophore onto skin (Fig. 2a), while the location of fluorescent layer under the base layer simulates subsurface accumulation of PS's (due to blood microcirculation) after intravenous injection (Fig. 2b).

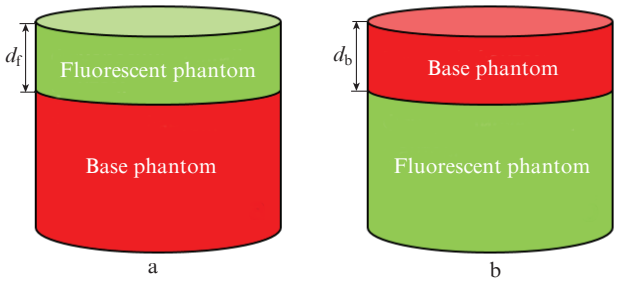

Figure 2. (Colour online) Schematic of two-layer agar phantoms of biotissue, which imitate (a) topical and (b) intravenous administration of a photosensitiser.

In this work, fluorescent properties were studied for two-layer phantom types corresponding to the configurations shown in Figs 2a and 2b; a 30-mm-thick phantom was chosen as the lower layer, and one of the phantoms with a thickness of 0.51–2.00 mm was chosen as the upper layer. Corresponding single-layer phantoms with the thickness of 30 mm were considered as the marginal cases of zero thickness of the upper layer. Thus, total thickness of the two-layer phantoms varied in the range of 30–32 mm.

2.2. Spectrophotometry measurements

In order to determine optical properties of the fabricated agar phantoms, measurements of collimated and diffuse transmission spectra, as well as diffuse reflection in the wavelength range of 370–1000 nm were performed using a Specord 250 Plus spectrophotometer (Analytik Jena, Germany) equipped with an integrating sphere. Samples of phantoms and their components were placed in quartz cuvettes with a thickness of 2 mm for measurements. The spectra of the absorption coefficient μ_a and the reduced scattering coefficient μ_s' were reconstructed from the results of spectrophotometric measurements of diffuse transmission and reflection spectra by the inverse Monte Carlo technique [26]. Absorption spectra of ink and water were determined from their collimated transmission spectra.

2.3. Fluorescence imaging

Fluorescence images of the fabricated agar phantoms of biotissue were acquired with a device for monitoring PS accumulation (IAP RAS, Russia) [8, 22, 27] equipped with two LED sources at wavelengths 405 ± 10 nm and 660 ± 10 nm synchronised with a CCD camera. Intensities of probing radiation on the surface of studied object were $I_{660}^{(0)} = 0.83$ W cm^{-2} and $I_{405}^{(0)} = 0.61$ W cm^{-2} for wavelengths of 660 and 405 nm, respectively. No optical filters were used during fluorescence excitation with the blue LED, since its emission spectrum is far from the PS fluorescence emission spectrum. Probing radiation of the red LED passes through a 641/75 filter (Semrock, USA). In order to exclude the effect of red probing radiation on the detected fluorescence signal, a 772/140 filter (Semrock, USA) was used in the registration system.

3. Results and discussion

The appearance of the produced agar biotissue phantoms is shown in Fig. 3. Fluorescent biotissue phantoms have a slightly greenish tint due to the presence of PS's in their composition. It should be noted that visually phantoms have a more intense colour as compared to human skin, since visually the skin colour is due to the optical properties of the superficial stratum corneum, which does not contain blood vessels, while macroscopic optical properties of skin are determined by the underlying layers containing blood vessels.

Absorption and scattering spectra of all components of the phantom (agar gel, red ink, lipofundin, and water) reconstructed from spectrophotometric measurements are shown in Fig. 4a. The concentrations of the substances used for measurements of individual spectra of phantom components correspond to those in the final phantom. Ink solution and water do not exhibit significant scattering, while absorption coefficient of lipofundin is determined primarily by water. The reconstructed reduced scattering coefficient of agar was found to be insignificant and is not shown in Fig. 4a. It should be noted that in accordance with obtained dependences, one can expect that scattering in the fabricated phantom will be governed by the presence of lipofundin, while absorption in wavelength range of 400–900 nm will be mainly due to red ink, and agar will provide a small contribution to the absorption in the blue spectral range. Prior to fabrication, a prediction of optical properties was made for the 'expected phantom' by summing scattering spectra of lipofundin and agar and, separately, partial absorption spectra of red ink solution

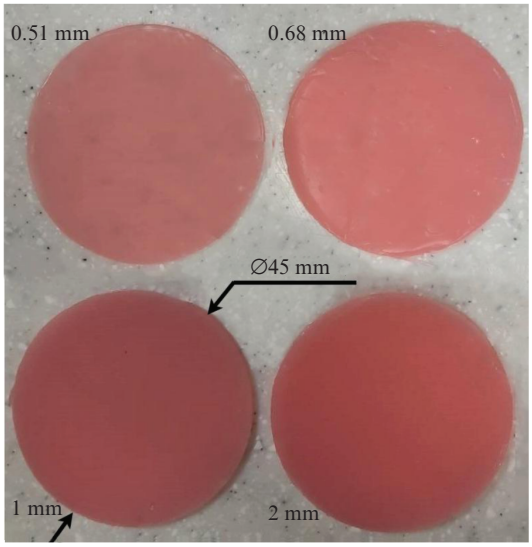

Figure 3. (Colour online) Agar phantoms of basic biotissue of various thicknesses (top view; the phantom thickness is shown in the figure).

and agar taken in relative concentrations corresponding to their content in the phantom. Figure 4b shows spectral dependences of optical properties of three compositions: (1)

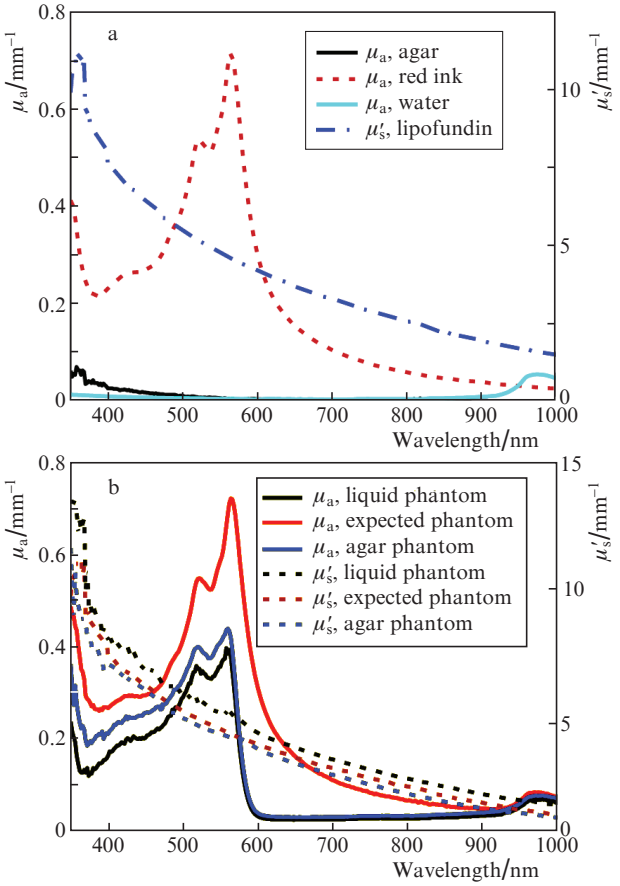

Figure 4. (Colour online) Spectral dependences of absorption coefficient and reduced scattering coefficient for phantom components (a); for agar phantom, liquid phantom consisting of lipofundin, red ink and water, and expected values calculated as the sum of the partial spectra of the individual components ('expected phantom') (b).

expected phantom; (2) liquid phantom consisting of lipofundin, red ink, and water (these main components are responsible for mimicking optical properties of biological tissues in the phantom); and (3) fabricated agar phantom. The spectra of the liquid phantom and the expected phantom differ both in amplitude and in characteristic shape (this concerns a sharper decrease in the absorption coefficient around 600 nm for a liquid phantom compared to the expected one), which is due to the interaction of ink and lipofundin. Presumably, ink nanoparticles stick to the droplets of soybean oil with a typical micron size when ink is added to lipofundin, which leads to a reduced content of ink particles in water and, accordingly, to lower absorption relative to the expected one. At the same time, droplets of soybean oil in a shell of ink nanoparticles also change their properties, which leads to a change in their scattering cross-section. Absorption in agar phantom is also lower than the expected one; however, it exceeds that for the liquid phantom, while scattering is close to expected values, which suggests that the effect of interaction between lipofundin and ink is lower in the agar phantom than that in the liquid phantom.

Figure 5 shows optical properties of phantoms of basic biotissue and biotissue with an added PS, reconstructed from the spectrophotometric measurements, in comparison with spectra of human skin *in vivo* averaged over different localisations [24]. Since in [24] the spectra of the scattering coefficient are presented, we used the value of anisotropy factor $g = 0.67$, which corresponds to the phase function used in this work, to calculate the reduced scattering coefficient. The presented data demonstrate that the fabricated phantoms provide good agreement with the optical properties of human skin in spectral range from 500 to 800 nm; however, in the range of 350–500 nm absorption of the resulting phantom is significantly lower than the values typical for real biotissues due to absorption of melanin and beta-carotene [28, 29]. Despite this discrepancy, it should be noted that absorption in this range significantly exceeds absorption in the red and near-IR ranges, which qualitatively repeats observed trends in biotissues, and such phantoms can be used for the testing of dual-wavelength fluorescence imaging techniques, which are based on significant difference in optical properties of biotissues in different spectral ranges [8, 22, 25, 30–32]. The deviation in the values of optical properties after the re-production of phantoms following the same protocol does not exceed 15%.

As can be seen from Fig. 5a, the addition of the PS practically does not affect the spectrum of the reduced scattering coefficient, while peaks around wavelengths of 405 and 660 nm are clearly visible in the absorption spectrum of the PS-containing phantom, which correspond to the peaks in absorption spectrum of the chlorin-based PS (Fig. 1). Absorption coefficients of basic and fluorescent phantoms coincide in the rest of the considered spectral range.

One of the important parameters of a phantom is its stability, which is the preservation of its optical properties over time. In order to test the stability of the produced phantom, we stored it for a month in a dry, dark place at a temperature of 4 °C wrapped in an airtight film. Figure 5c shows the results of the calculation of relative changes in optical properties of the phantom one month after production:

$$\delta\mu_a = \frac{\mu_{a2} - \mu_{a1}}{(\mu_{a2} + \mu_{a1})/2}, \quad \delta\mu_s' = \frac{\mu_{s2}' - \mu_{s1}'}{(\mu_{s2}' - \mu_{s1}')/2},$$

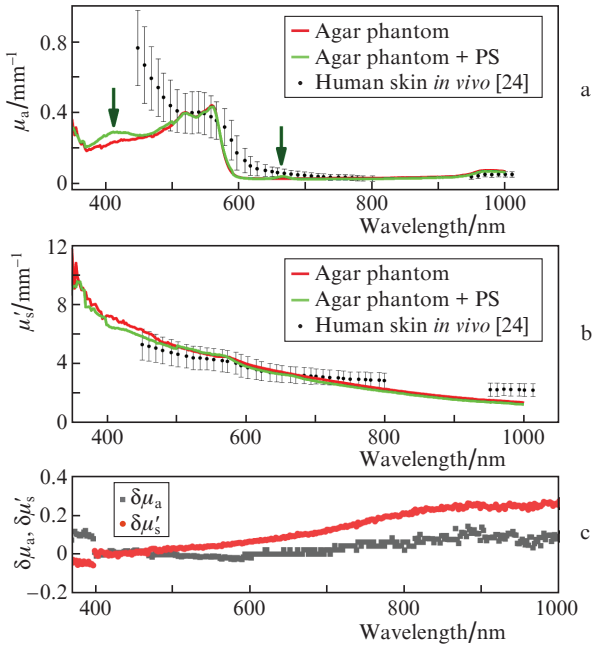

Figure 5. (Colour online) Reconstructed spectra of (a) the absorption coefficient and (b) reduced scattering coefficient of agar phantoms of basic biotissue (agar phantom) and biotissue with chlorin-based PS administration (agar phantom + PS) in comparison with the averaged spectra of human skin *in vivo* from [24]. Green arrows show absorption peaks of the PS. (c) Relative changes in the reduced scattering coefficient and absorption coefficient of the phantom after 1 month.

where subscript 1 corresponds to the phantom immediately after production, and subscript 2 corresponds to the phantom after 1 month. The results demonstrate insignificant (within 25%) increase in reduced scattering coefficient and absorption coefficient (and the deviation do not exceed 10% in the wavelength range of 500–700 nm), which is associated with a slight evaporation of water from the phantom during storage.

Figure 6 shows fluorescence images of produced single-layer phantoms of biotissue with the thickness of 30 mm upon fluorescence excitation at wavelengths of 405 nm and 660 nm, corresponding to absorption peaks of the chlorin-based PS, while the registration of fluorescence emission was performed in the vicinity of the wavelength of 760 nm. The images are presented in the form of maps of fluorescence intensities I_{405} and I_{660} registered by the CCD-camera in bit units (the subscript corresponds to the excitation wavelength). The intensities are normalised to corresponding values of the probing intensities $I_{405}^{(0)}$ and $I_{660}^{(0)}$.

Fluorescence images of phantoms of basic biotissue and biotissue with the added PS are shown in the same colourmap for both fluorescence excitation wavelengths. Thus, Fig. 6 clearly demonstrates that the fluorescence of phantoms is due to the addition of the PS, rather than to the autofluorescence of components included both to the basic and fluorescent phantoms.

Figure 7 shows the dependences of averaged fluorescence signals from two-layer phantoms, which imitate the cases of topical application and intravenous injection of the PS (Fig. 2), on the thickness of the upper fluorescent layer d_f or the upper basic layer d_b. The region of fluorescence signal averaging is shown in Fig. 6 as a solid line. A monotonic increase in fluorescence signal in the case of simulating topical application (Fig. 7a) is caused by an increase in the thickness

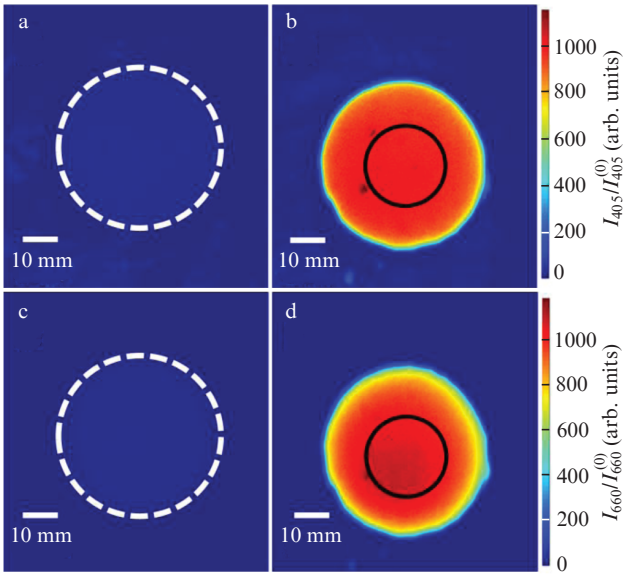

Figure 6. (Colour online) Fluorescence images of phantoms of (a, c) the basic biotissue (boundaries of phantom are indicated by dashed lines) and (b, d) biotissue with chlorin-based PS administration obtained upon fluorescence excitation at wavelengths of (a, b) 405 and (c, d) 660 nm. Solid lines show the averaging area for the calculation of fluorescence signals from phantoms.

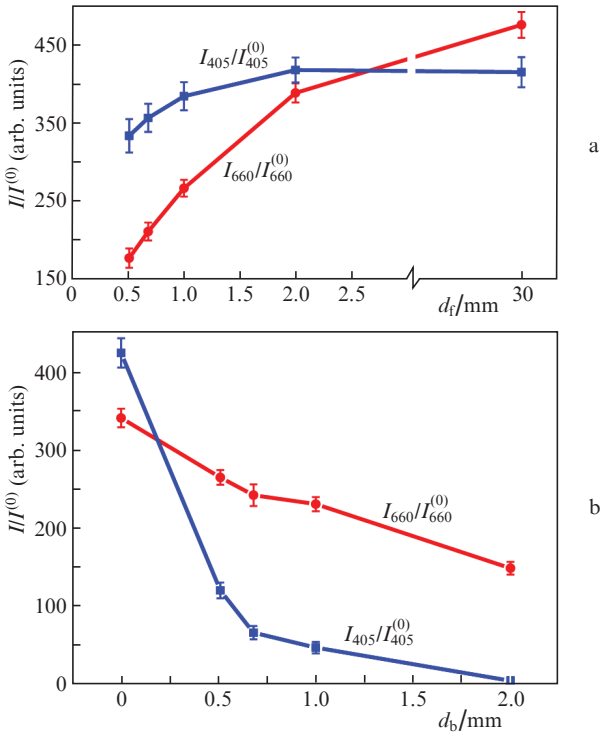

Figure 7. Experimental dependences of fluorescence signals $I_{660}/I_{660}^{(0)}$ and $I_{405}/I_{405}^{(0)}$ corresponding to excitation wavelengths of 660 and 405 nm and normalised to the corresponding intensities of probing radiation on the thickness of upper layer obtained for two-layer agar phantoms of biotissue which imitate (a) topical and (b) intravenous administration of a photosensitiser.

of the PS-containing layer and, consequently, in total amount of the PS in the phantom. Asymptotic tendency of this dependence to a constant level is due to the fact that with an increase in the thickness of fluorescent layer to the penetration depth of probing radiation, a further increase in its thickness will not affect the value of the detected fluorescence signal. A monotonous decrease in the fluorescence signal in the case of simulating intravenous administration (Fig. 7b) is due to an increase in the attenuation of exciting radiation in the upper layer, which does not contain a PS, with an increase in its thickness.

Quantitative differences in the dynamics of normalised fluorescence signals $I_{405}/I_{405}^{(0)}$ and $I_{660}/I_{660}^{(0)}$ corresponding to excitation wavelengths of 405 nm and 660 nm are determined by the difference in optical properties of basic biotissue phantom: stronger absorption and scattering of light in blue wavelength range leads to larger attenuation of the exciting radiation at 405 nm compared to 660 nm, and, as a result, the fluorescence signal for excitation in the red wavelength range is larger than that at 405 nm for large thicknesses of the upper layer. On the other hand, for small thicknesses of the upper fluorescent layer d_f, attenuation at the wavelength of 405 nm is compensated by higher intrinsic absorption of the PS compared to absorption at the wavelength of 660 nm (see Fig. 1). As a result, the fluorescence signal upon excitation at 405 nm is larger than that at 660 nm. The effect of biotissue optical properties on the registered fluorescence signals is discussed in detail elsewhere [25, 32].

Previously in [25], we proposed an analytical model of signal formation in dual-wavelength fluorescence imaging and demonstrated that the ratio of normalised fluorescence signals at two excitation wavelengths

$$R_\lambda = \frac{I_{660}/I_{660}^{(0)}}{I_{405}/I_{405}^{(0)}}$$

allows the fluorophore localisation depth to be estimated. Figure 8 shows measured ratios R_λ of fluorescence signals corresponding to excitation wavelengths of 660 and 405 nm, for the fabricated two-layer phantoms, as well as corresponding analytical dependences derived from analytical models developed in [25] for the cases of fluorophore presence in upper or lower layers for the biotissue optical properties shown in Fig. 5. The ratio R_λ obtained from experimental data was additionally normalised to the ratio of fluorophore absorption peaks obtained by the registration of fluorescence images of a test object represented by a thin layer of a dried PS deposited on a black substrate. The asymptotic saturation of the considered R_λ value for the case which imitates topical application of the PS (Fig. 8a), similar to the dependences for the signals (Fig. 7a), is explained by the limited probing depth of the fluorescence imaging technique, when variation in the fluorophore content at large depths does not affect the measured value of the fluorescence signal. An exponential increase in the value of R_λ for the case imitating intravenous injection of the PS (Fig. 8b) is explained by an exponential decay of exciting radiation at both wavelengths, and for the 405-nm wavelength the attenuation coefficient is significantly higher. All observed dependences qualitatively repeat the dependences obtained in [25] for other values of phantom optical properties.

4. Conclusions

The paper proposes a simple and cost-effective approach to fabrication of agar phantoms that mimic optical properties of biotissue before and after chlorin-based PS administration.

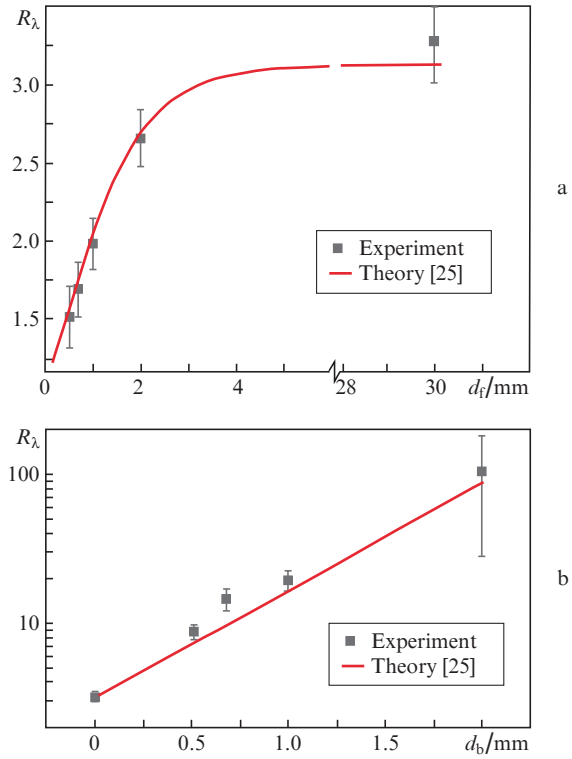

Figure 8. (Colour online) Experimental dependences of ratio R_λ of fluorescence signals corresponding to the excitation wavelengths of 660 nm and 405 nm on the thickness of upper layer obtained for two-layer agar phantoms of biotissue imitating topical (a) and intravenous (b) administration of a photosensitiser, and corresponding analytical dependencies obtained using the analytical model presented in [25].

Fluorescent properties of the phantoms and differences in absorption spectrum are determined exclusively by the presence of a PS, rather than by the autofluorescence of individual components of the phantom. The effect of the PS on the spectrum of the reduced scattering coefficient is demonstrated to be insignificant. In order to maintain stability, phantoms should be stored under conditions that prevent drying (for example, in an airtight film in a fridge).

The proposed approach allows fabricating multilayer phantoms of biotissue that imitate various ways of PS administration, which is important for model experiments on fluorescence imaging for planning and monitoring of PDT with the chlorin-based PS.

Acknowledgements. This work was supported by the Russian Science Foundation (Project No. 17-15-01264). The authors are grateful to V.V. Perekatova for assistance in the production of phantoms and Revixan Ltd for providing a photosensitiser for the experiment.

References

1. Diao S., Blackburn J.L., Hong G., Antaris A.L., Chang J., Wu J.Z., Zhang B., Cheng K., Kuo C.J., Dai H. *Angew. Chem.*, **127** (49), 14971 (2015).
2. Kim C., Song K.H., Gao F., Wang L.V. *Radiology*, **255** (2), 442 (2010).
3. Canpolat M., Mourant J.R. *Appl. Opt.*, **39** (34), 6508 (2000).
4. Kim C., Garcia-Uribe A., Kothapalli S.-R., Wang L.V. *Proc. SPIE*, **6870**, 68700M (2008).
5. Lepore M., Delfino I. *Open Biotechnol. J.*, **13** (1), 163 (2019).
6. Di Ninni P., Martelli F., Zaccanti G. *Phys. Med. Biol.*, **56** (2), 21 (2010).
7. Krainov A., Mokeeva A., Sergeeva E., Agrba P., Kirillin M.Y. *Opt. Spectrosc.*, **115** (2), 193 (2013).
8. Khilov A., Kirillin M., Loginova D., Turchin I. *Laser Phys. Lett.*, **15** (12), 126202 (2018).
9. Di Ninni P., Bérubé-Lauzière Y., Mercatelli L., Sani E., Martelli F. *Appl. Opt.*, **51** (30), 7176 (2012).
10. Waterworth M., Tarte B., Joblin A., van Doorn T., Niesler H. *Australas. Phys. Eng. Sci. Med.*, **18** (1), 39 (1995).
11. Royston D.D., Poston R.S., Prahl S.A. *J. Biomed. Opt.*, **1** (1), 110 (1996).
12. Madsen S.J., Patterson M.S., Wilson B.C. *Phys. Med. Biol.*, **37** (4), 985 (1992).
13. Di Ninni P., Martelli F., Zaccanti G. *Opt. Express*, **18** (26), 26854 (2010).
14. Loginova D.A., Sergeeva E.A., Krainov A.D., Agrba P.D., Kirillin M.Yu. *Quantum Electron.*, **46** (6), 528 (2016) [*Kvantovaya Electron.*, **46** (6), 528 (2016)].
15. Spinelli L., Botwicz M., Zolek N., Kacprzak M., Milej D., Sawosz P., Liebert A., Weigel U., Durduran T., Foschum F. *Biomed. Opt. Express*, **5** (7), 2037 (2014).
16. Mustari A., Izumi Nishidate M., Wares A., Maeda T., Kawauchi S., Sato S., Sato M., Aizu Y. *J. Vis. Exp.*, **138**, 57578 (2018).
17. Ntombela L., Adeleye B., Chetty N. *Heliyon*, **6** (3), e03602 (2020).
18. Lamouche G., Kennedy B.F., Kennedy K.M., Bisaillon C.-E., Curatolo A., Campbell G., Pazos V., Sampson D.D. *Biomed. Opt. Express*, **3** (6), 1381 (2012).
19. Shupletsov V.V., Zherebtsov E.A., Dremin V.V., Popov A.P., Bykov A.V., Potapova E.V., Dunaev A.V., Meglinsky I.V. *Quantum Electron.*, **51** (2), 118 (2021) [*Kvantovaya Electron.*, **51** (2), 118 (2021)].
20. Spikes J.D. *J. Photochem. Photobiol. B: Biol.*, **6** (3), 259 (1990).
21. Ol'shevskaya V.A., Nikitina R.G., Savchenko A.N., Malshakova M.V., Vinogradov A.M., Golovina G.V., Belykh D.V., Kutchin A.V., Kaplan M.A., Kalinin V.N. *Bioorg. Med. Chem.*, **17** (3), 1297 (2009).
22. Kirillin M., Kurakina D., Khilov A., Orlova A., Shakhova M., Orlinskaya N., Sergeeva E. *Biomed. Opt. Express*, **12** (2), 872 (2021).
23. Kurakina D., Khilov A., Shakhova M., Orlinskaya N., Sergeeva E., Meller A., Turchin I., Kirillin M. *J. Biomed. Opt.*, **25** (6), 063804 (2019).
24. Kono T., Yamada J. *Int. J. Thermophys.*, **40**, 51 (2019).
25. Kirillin M., Khilov A., Kurakina D., Orlova A., Perekatova V., Shishkova V., Malygina A., Mironycheva A., Shlivko I., Gamayunov S. *Cancers*, **13** (22), 5807 (2021).
26. Zabotnov S.V., Skobelkina A.V., Sergeeva E.A., Kurakina D.A., Khilov A.V., Kashaev F.V., Kaminskaya T.P., Presnov D.E., Agrba P.D., Shuleiko D.V. *Sensors*, **20** (17), 4874 (2020).
27. Kleshnin M., Fiks I., Plekhanov V., Gamayunov S., Turchin I. *Laser Phys. Lett.*, **12** (11), 115602 (2015).
28. Zonios G., Dimou A., Bassukas I., Galaris D., Tsolakidis A., Kaxiras E. *J. Biomed. Opt.*, **13** (1), 014017 (2008).
29. Meredith P., Sarna T. *Pigment Cell Res.*, **19** (6), 572 (2006).
30. Shakhova M., Loginova D., Meller A., Sapunov D., Orlinskaya N., Shakhov A., Khilov A., Kirillin M. *J. Biomed. Opt.*, **23** (9), 091412 (2018).
31. Khilov A.V., Kurakina D.A., Turchin I.V., Kirillin M.Yu. *Quantum Electron.*, **49** (1), 63 (2019) [*Kvantovaya Electron.*, **49** (1), 63 (2019)].
32. Khilov A.V., Sergeeva E.A., Kurakina D.A., Turchin I.V., Kirillin M.Yu. *Quantum Electron.*, **51** (2), 95 (2021) [*Kvantovaya Electron.*, **51** (2), 95 (2021)].